4MOST low resolution spectrograph performances

Karen Disseau, Didier Boudon, Diane Chapuis, Eric Daguisé, Aurélien Jarno, Alexandre Jeanneau, Jens-Kristian Krogager, Florence Laurent, Matthew Lehnert, Jean-Emmanuel Migniau, et al.

4MOST Low Resolution Spectrograph Performances

Karen Disseau*[a], Didier Boudon[a], Diane Chapuis[a], Eric Daguisé[a], Aurélien Jarno[a], Alexandre Jeanneau[a], Jens-Kristian Krogager[a], Florence Laurent[a], Matthew Lehnert[a], Jean-Emmanuel Migniau[a], Arlette Pécontal[a], Emmanuel Pécontal[a], Alban Remillieux[a], Johan Richard[a]

[a]Univ Lyon, Univ Lyon1, Ens de Lyon, CNRS, Centre de Recherche Astrophysique de Lyon UMR5574, F-69230, Saint-Genis-Laval, France

ABSTRACT

4MOST, the 4m Multi Object Spectroscopic Telescope, is an upcoming optical, fiber-fed, MOS facility for the VISTA telescope at ESO's Paranal Observatory in Chile. Its main science drivers are in the fields of galactic archeology, high-energy physics, galaxy evolution and cosmology. The 4MOST consortium consists of several institutes in Europe and Australia under the leadership of the Leibniz-Institut für Astrophysik Potsdam (AIP). 4MOST is currently in its Assembly, Integration and Tests Phase with an expected start of science operations in 2023. The design of 4MOST features 2436 fibers split into two low-resolution spectrographs (1624 fibers, 370-950 nm, R > 4000) and a high-resolution spectrograph (812 fibers, ~44-69 nm coverage, R > 18000). A fiber positioner covers a hexagonal field of view of ~4.1 deg².
CRAL has the full responsibility of the Low Resolution Spectrographs. Each of them is composed of an off-axis collimator collecting the f/3 beam coming from the fibers and providing a 200 mm collimated beam, which is then split into three arms thanks to two dichroics. Each arm is composed of a Schmidt corrector, a VPHG, an f/1.73 camera and a standard 6k by 6k 15µm pixel detector.
Manufacturing, Assembly, Integration and Test (MAIT) phase of the LRS started in May 2018. The first LRS has now been fully integrated, aligned and tested and its Local Acceptance Review on site at CRAL passed successfully in December 2021. This paper describes the procedures developed to test the spectrograph and demonstrate its compliance with the requirements. Performances achieved are presented throughout the paper, especially in terms of spectral resolving power and sampling, spectral purity, cross-talk, throughput, straylight, light tightness and stability.

Keywords: 4MOST, VISTA, Low Resolution Spectrograph, Multi-Object Spectroscopy, Fiber-fed spectrograph, Manufacture, Assembly, Integration and Test.

1. INTRODUCTION

4MOST is a wide-field, high multiplex, fiber-fed optical spectroscopic survey facility to be mounted on the 4-m telescope VISTA of the European Southern Observatory (ESO). With its large enough field-of-view to survey a large fraction of the southern sky in a few years, the facility will be able to simultaneously obtain spectra of ~2400 objects distributed over a hexagonal field of view of 4.2 square degrees. It enables many science goals, in the field of galactic archeology, high energy physics, galaxy evolution and cosmology, and its design complements a number of key all-sky, space-based observatories of prime European interest (Gaia, eRosita, Euclid and PLATO) and future ground-based, wide area survey facilities like the Vera C. Rubin Observatory and SKA [1].

The instrument features a Wide Field Corrector, which provides a nearly un-vignetted image of 2.6 degrees diameter in the focal surface of the telescope (at the conventional Cassegrain focus), and an Atmospheric Dispersion Corrector that corrects for atmospheric dispersion up to 55 degrees zenith distance [2]. A fiber positioning system based on the tilting spine principle can simultaneously position the 2436 science fibers that are arranged in a hexagonally shaped grid at the focal surface [3]. The fiber-feed subsystem [4] then transports light from the focal surface to the slits of the three 4MOST spectrographs: 1624 fibers go to the two Low Resolution Spectrographs with R>4,000 and 812 fiber go to the High Resolution Spectrograph [5] with R>18,000.

*karen.disseau@univ-lyon1.fr; phone 33 478 868 527; http://cral.univ-lyon1.fr/

The two Low Resolution Spectrographs were built in Lyon at CRAL, and the first one has now been fully integrated, aligned and tested: after passing successfully its local acceptance review in December 2021, it was dismounted and shipped to AIP in March 2022, where it was re-integrated and tested.

This paper focuses on the performances of the first LRS and the procedures developed to test it and demonstrate its compliance with the requirements. Section 2 gives a quick overview of the spectrograph design and the main performance requirements. Section 3 summarizes the tools that are used to illuminate the LRS slit during the verification phase at CRAL. Test processes and results are detailed in section 4. Section 5 finally concludes the paper with upcoming LRS integration and verification phase.

2. 4MOST LRS DESIGN OVERVIEW AND KEY REQUIREMENTS

The Low Resolution Spectrograph (LRS) is composed of 2 symmetrical unit spectrographs including the same optical components. Each spectrograph is fed by an entrance slit of 812 fibers following the focal plane curvature radius. A slit lens is glued onto the slit fibers. A spherical mirror collects the F/3 light coming from the fibers and generates a collimating beam of 200 mm. Two dichroics split the beam into three channels: blue, green, red. Each channel is composed of the same optical elements: a Schmidt corrector, a Volume-Phase Holographic Grating (VPHG) for dispersion, a dioptric camera and a Field Lens Window. A 6k x 6k detector with 15µm pixel records the spectra. Figure 1 shows the optical and mechanical model of the LRS.

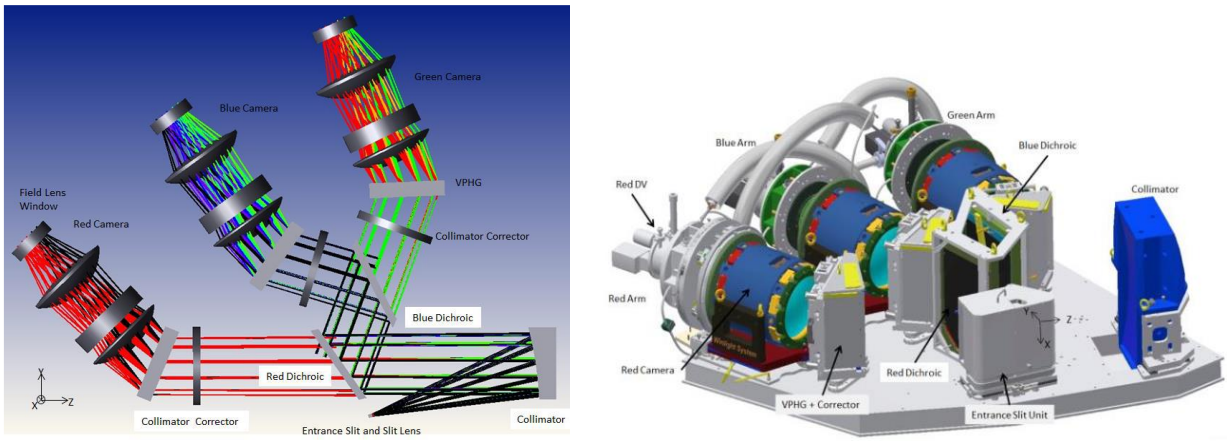

Figure 1. LRS Optical layout (left) and mechanical model (right).

The LRS key requirements are derived from the 4MOST top level requirements ([7] and [8]). The paper focuses on the verification of the functional and performance requirements listed below, which are all verified by test:

1. The LRS shall be able to accommodate a minimum of 812 science fibers and 10 calibration fibers. It shall accept an input f/3.0 beam, with 85 µm micron core diameter fiber. The LRS shall cover simultaneously the wavelength range from 400 nm to 885 nm, with a goal from 370 nm to 950 nm. The dichroic transition region shall not include the wavelength ranges 428.3 – 432.1 nm (G-band), 514-520 nm (Mgb triplet) and 648-666 nm (Hα 656.2 nm).
2. The LRS resolving power shall be $R \geq 10 \times \lambda$ for $400\ nm \leq \lambda < 500\ nm$ and $R \geq 5000$ for $500\ nm \leq \lambda \leq 850\ nm$. At any wavelength, the variation of the LRS spectral resolution shall not exceed 20% PTV over each individual detector.
3. The LRS sampling shall be ≥ 2.5 pixels (with a goal of 3.0 pixels). The variation of the LRS sampling shall be < 50% PTV over each individual detector.
4. Spectral purity: a custom fit function (explained in detail in section 4.1) fitted to an unresolved emission line shall contain 85% (goal 90%) of the emission line's total flux within ±FWHM from its center. The requirement must be fulfilled over 95% (goal 99%) of the detector area.

5. Cross-talk: At any given wavelength and at all spectra locations, no spectrum shall contaminate its neighboring spectra on the detector with more than 2% (goal 1%) of its own flux. The requirement must be fulfilled over 95% (goal 99%) of the detector area.
6. Stray light and ghosts: The spectrograph shall limit the intensity of the diffuse scattered light on the detector at any wavelength to less or equal than 3% (goal 1%) of the mean intensity of the source light at any wavelength. The spectrograph shall also limit the intensity of any ghost image to less than 0.2% (goal 0.1%) of the intensity of the parent image.
7. Light tightness: The spectrograph shall limit the increase of the background signal at the detector by additional light sources to 3e-/hour/pixel by night and 100 e-/hour/pixel during day time with dome lights on.
8. Spectrograph stability: The LRS shall be mechanically and thermos-elastically stable enough to ensure a maximum displacement of fiber core image on the detector of 1.5 µm over 1 hour in spectral and spatial direction and in the VISTA environment conditions.
9. Throughput and homogeneity of spectral response: the LRS throughput, defined as the percentage of light available at the exit of the fiber slit surface that is delivered to the detector, shall be greater than 50% at any wavelength. The variation in spectral response shall not exceed 10% (goal 5%) PTV.

The spectral resolving power and sampling requirements, directly related to the image quality, are checked right after each channel alignment as first verifications (health-checks) intended to validate the alignment. Then specific tests such as throughput, ghosts and stray light are performed (second verification). These tests are repeated during the third verification step performed on the whole LRS, once covers are closed, with other global tests such as light tightness and spectrograph stability.

3. LRS FIBERS ILLUMINATION

A full description of the tools used for the LRS verification can be found in [9]. Only a summary of the tools related to the fiber illumination is given here for a better understanding of the paper content.

The whole LRS MAIT phase were performed with a Test Slit Unit, hosting a partially populated slit. The slit box is thus composed of only 6 slitlets (shown in yellow in Figure 2), which are themselves only sparsely populated with 11 fibers each, 6 colored in blue and 5 colored in red in Figure 2. Only the population scheme of the slit with the fibers colored in red is used to perform the test described throughout the paper.

The Light Source Module is composed of the light sources connected via liquid light guides to an illumination unit, which injects light at the proper f-ratio into the bundle of fibers. The light sources are a Quartz-Tungsten-Halogen (QTH) lamp for the continuum source and Pencil Hg and Ne lamps for calibration arc lamps.

An example of the full detector image of the fiber spectra, with arc lamp and continuum lamp, is given in Figure 3.

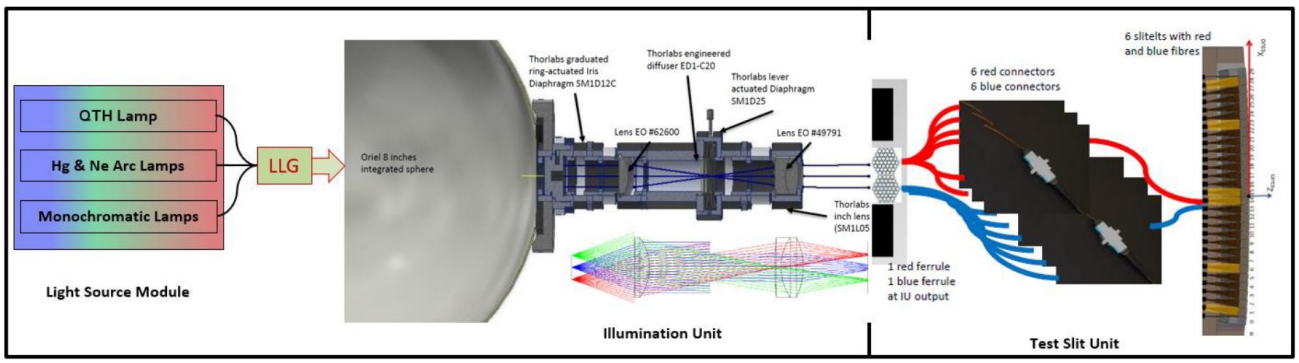

Figure 2. Illumination of the LRS Test Slit Unit with the light sources and illumination unit.

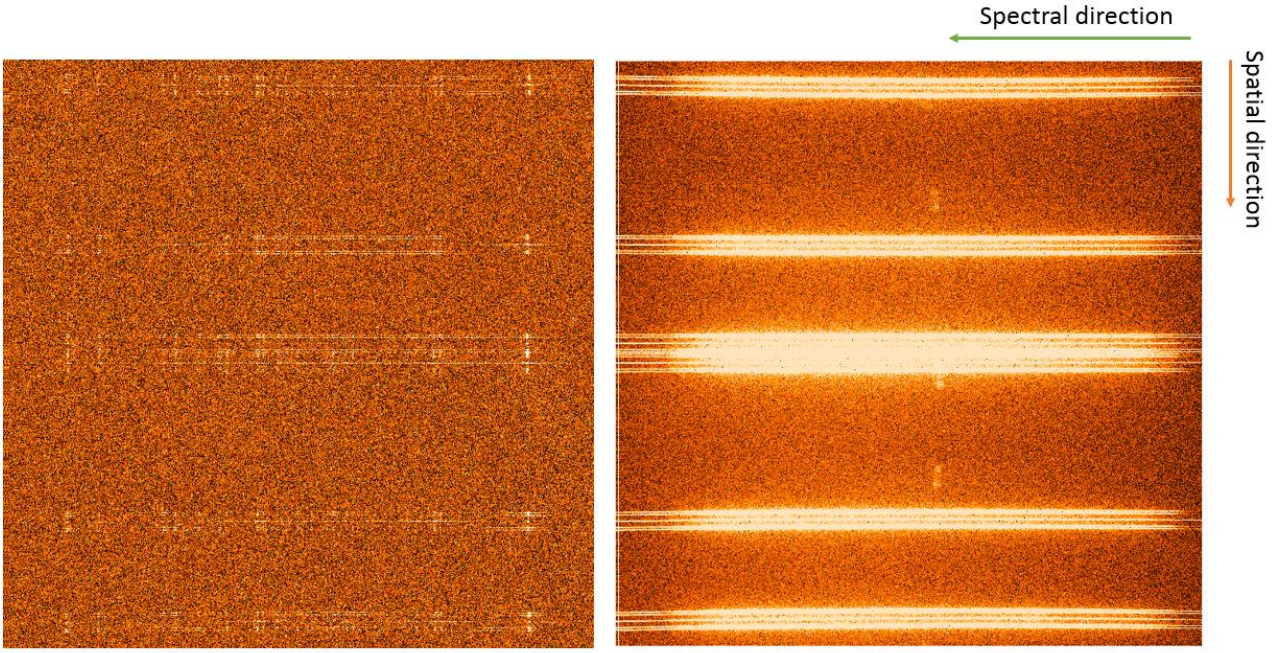

Figure 3. Example of arc (Ne lamp) exposure (left) and continuum (QTH lamp) exposure in the green channel. The detector image shows the spectral dispersion (from the right for the bluer part to the left for the reddest part here) of each fiber (6 slitlets of 5 fibers populating the Test Slit Unit).

4. LRS PERFORMANCES

Every software needed to analyze the spectra obtained with the LRS, and compute the numerous criteria presented hereafter, were developed at CRAL by our software team.

4.1 Spectral resolving power and sampling

The LRS Test Slit Unit is illuminated, through the Light Source Module, with Arc lamps (Hg lamp for the blue channel and Ne lamp for the green and red channels). First a series of 10 bias is taken and a master bias is created by computing the median of the 10 bias exposures. Arc lamp exposures are then taken and bias-subtracted with the master bias.

Exposure analysis is performed as follows:

- The dispersion solution is measured from the spectral line identified in the central set of fibers. A 1D Gaussian is fitted in each line and the pixel locations are compared with the reference wavelengths from the Hg and Ne catalogs to provide the law $\lambda = f(\text{pixel})$ for each LRS channel.
- For each line, the Line Spread Function (LSF) is modelled using a custom model. A fiber model, obtained by creating an ellipse of given axis length (given by the assumed fiber image size onto the detector), is convolved with a PSF modelled as a 2D Gaussian parametrized by its Full Width at Half Maximum (FWHM). The convolved circle is then rescaled using the detector pixel size (15 µm) and summed up over 5 pixels in the spatial direction. The best model is found by minimizing the difference between this model and the detector data, using a Least Square Fitting algorithm.
- Spectral resolving power and spectral sampling: the value of FWHM found for the best fitted model gives the size of a resolution element. The size in pixels of FWHM is the spectral sampling. The spectral resolving power R is then defined as the ratio λ/FWHM.

- Spectral resolving power and sampling variations: in each channel, the variation of R (resp. FWHM) is defined as the ratio of the difference between the maximum and minimum values of R (resp. FWHM) in spectral bins of 2 nm width to the average value of R (resp. FWHM) in the considered bin.

The FWHM map over the detector area as well as the spectral resolving power and spectral sampling as a function of wavelength, are shown for each channel in Figure 4. The dashed lines on the spectral resolving power and sampling plots shows the dichroic transition region (determined as explained in section 4.3).

Variations of spectral resolving power and sampling are shown in Figure 5 and Figure 6.

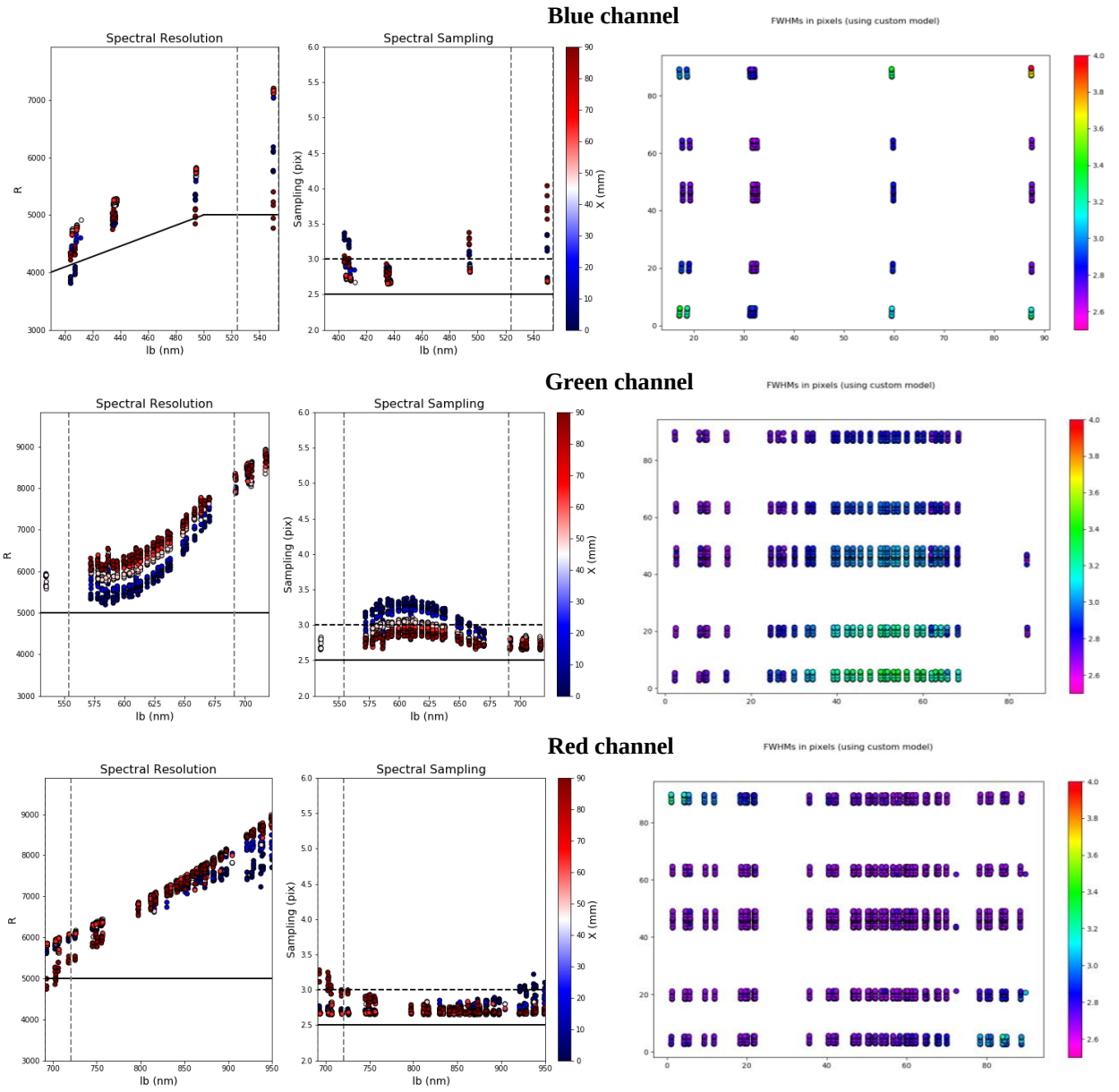

Figure 4. Left panels: Spectral resolving power and spectral sampling as functions of wavelength. The color bar shows the location along the spatial direction onto the detector. Vertical gray dashed lines shows the dichroic transition region. Right panels: FWHM maps computed thanks to the custom model on the detected lines. Vertical axis is the spatial direction and horizontal axis is the spectral direction, from blue on the left to red on the right for the blue and red channels, and the opposite for the green channel.

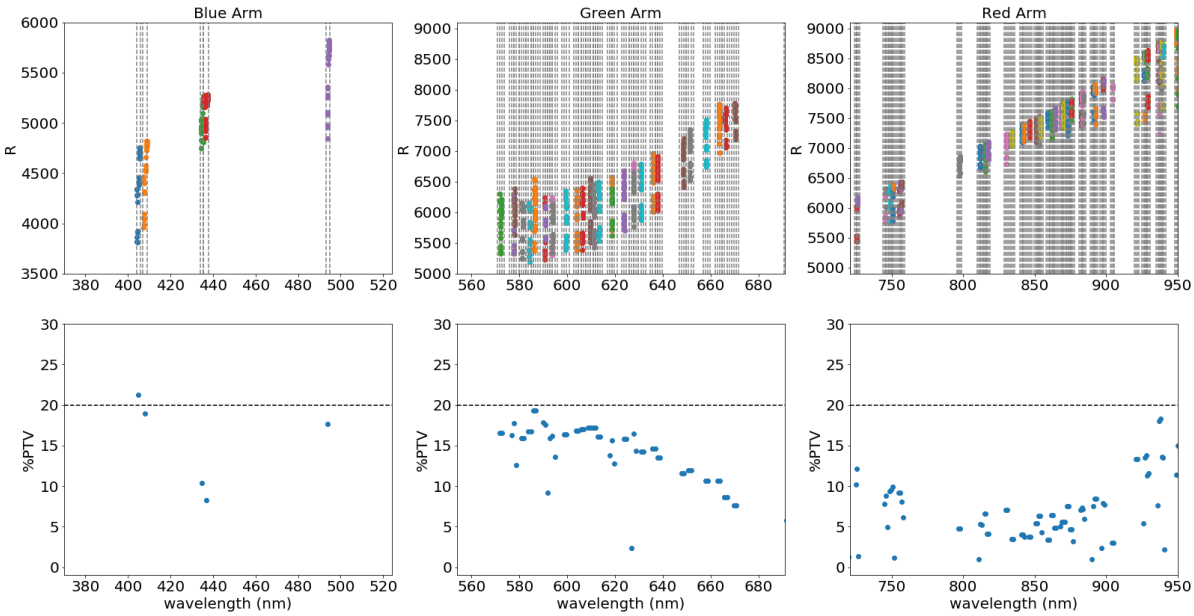

Figure 5. Spectral resolving power variations for each channel. Horizontal dashed line shows the specified limit.

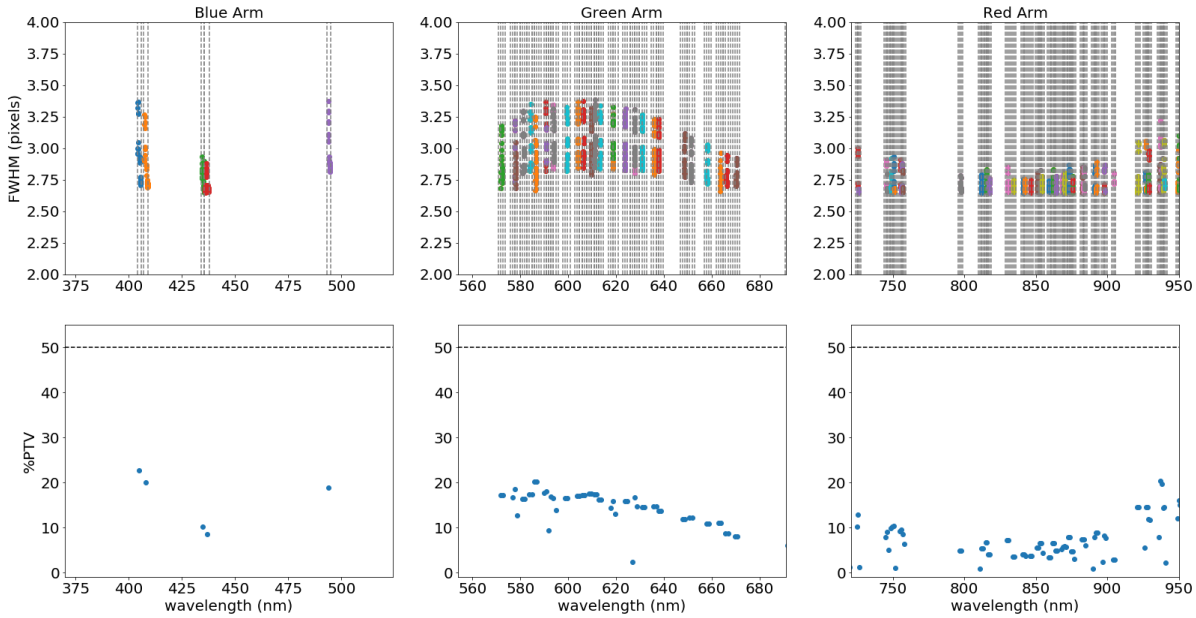

Figure 6. Spectral sampling variations for each channel. Horizontal dashed line shows the specified limit.

We observe in the blue and green channels some points out of specification in terms of spectral resolving power and its variation: there is obviously a slight degradation of the FWHM and spectral resolving power towards the detector bottom (this trend is clear in the green channel, as we can see in Figure 4, middle panel), due to a tilt residual on the DV w.r.t. the camera. During the alignment process, the adjustment of the detector tip/tilt [9] was the most difficult part: with experience, we improved the process for the other channels on LRS-A and LRS-B, and get better results on the PSF uniformity over the detector area.

Non-conformance reports were submitted to the Project Office for the Local Acceptance Review of the spectrograph, since this discrepancy could affect the uniformity of 4MOST science spectra across the 4MOST field of view. This impact is however limited since it concerns only a few wavelengths. This non-compliance was thus accepted, and further analysis will be performed at system level using the final science pipeline to recalculate the spectral resolution.

4.2 Spectral purity

The spectral purity criterion is checked on arc exposures: for each line onto the detector, it is defined as the ratio of the flux of the LSF curve summed over 5 pixels to the flux of the LSF curve integrated in the window [-FWHM, +FWHM] around the center. Values of spectral purity obtained for each detected line (each PSF) are plotted in Figure 7. Mean purity values are 96.75%, 99.92% and 99.63% in the blue, green and red channels respectively. In the green and red channels, all the calculated values are above the goal (90%), while in the blue channel, 99% of the points are above the specification (85%). The requirement is thus met in the blue over 95% of the detector area, as specified.

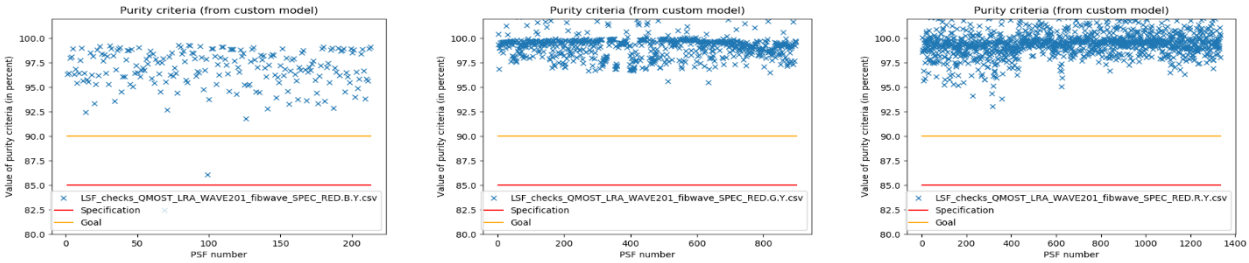

Figure 7. Spectral purity for the three channels: blue (left), green (middle), red (right). The horizontal red line shows the specified value, and the yellow line shows the goal.

4.3 Wavelength range and dichroic transition region

The LRS Test Slit Unit is illuminated with the QTH continuum lamp. Exposures are taken and bias-subtracted with a master-bias built as the median of a series of 10 bias frames.

The spectrum of the top, central and bottom fibers are extracted and calibrated in wavelength using the dispersion law obtained from arc exposures.

- Wavelength range: we measure the minimum and the maximum wavelengths where significant flux (>1% throughput, as computed in section 4.6) is detected in each channel. The bluest detected wavelength is 372 nm and the reddest one is 950 nm, which meets the requirement (400-885 nm) and is even very close to the goal (370-950 nm).
- Dichroic transition region: defining T(λ), TB(λ), TG(λ), TR(λ) the overall absolute transmission of LRS and the blue, green and red channels respectively, we have T(λ) = TB(λ)+TG(λ)+TR(λ). The dichroic transition region is measured at the wavelengths where T-TB > 1% and T-TG > 1% for the blue dichroic, and T-TG > 1% and T-TR > 1% for the red dichroic. The first transition between the blue and green channels is 524-554 nm and the second one between the green and red channels is 691-721 nm, which excludes as required the G-band, Mgb triplet and Hα line at 656.2 nm

4.4 Cross-talk between spectra

The cross-talk criterion is computed from the continuum lamp exposures. It is derived by computing the ratio of the flux contained in a 3x3 pixels box centered in the PSF to the flux contained in the same box separated by 6.5 pixels along the spatial direction.

Results are plotted in Figure 8. Mean values of cross-talk are 0.56%, 0.33% and 0.55% in the blue, green and red channels respectively. For all channels, 100% of the computed values are below the 2% specified, and more than 98% below the goal (1%).

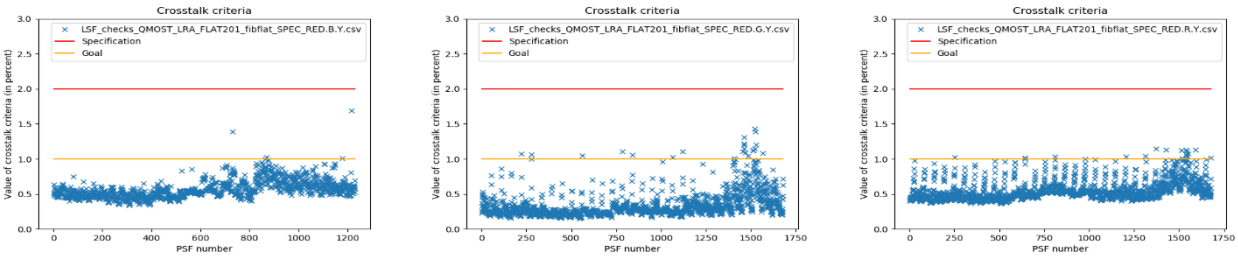

Figure 8. Cross-talk for the three channels: blue (left), green (middle), red (right). The horizontal red line shows the specified value, and the yellow line shows the goal.

4.5 Stray light and Ghosts

The continuum QTH lamp is used to illuminate half a field (limited either to the top three or the bottom three slitlets). Each set of exposures is composed of a non-saturated exposure and a saturated exposure. All exposures are bias subtracted using a master bias created as the median of a series of 10 bias exposures.

We compute the relative flux between the maximum diffuse light measured in the saturated exposures across the non-illuminated part of the detector (excluding Littrow ghosts) and the mean expected flux level scaled from the non-saturated exposures to cover the full detector. This relative flux are found to be lower than 0.1% in each channel, which is lower than the goal value of 1%.

Littrow ghosts (particularly visible in the blue, as shown in Figure 9) are identified and associated with their parent light from both sets of exposures. We compute the total integrated flux of each ghost and measure their flux ratio relative to the integrated flux of the parent light. The flux ratio is found to be <0.06% in the blue, and <0.02% in the green and red channels. This is again much lower than the goal value of 0.1%.

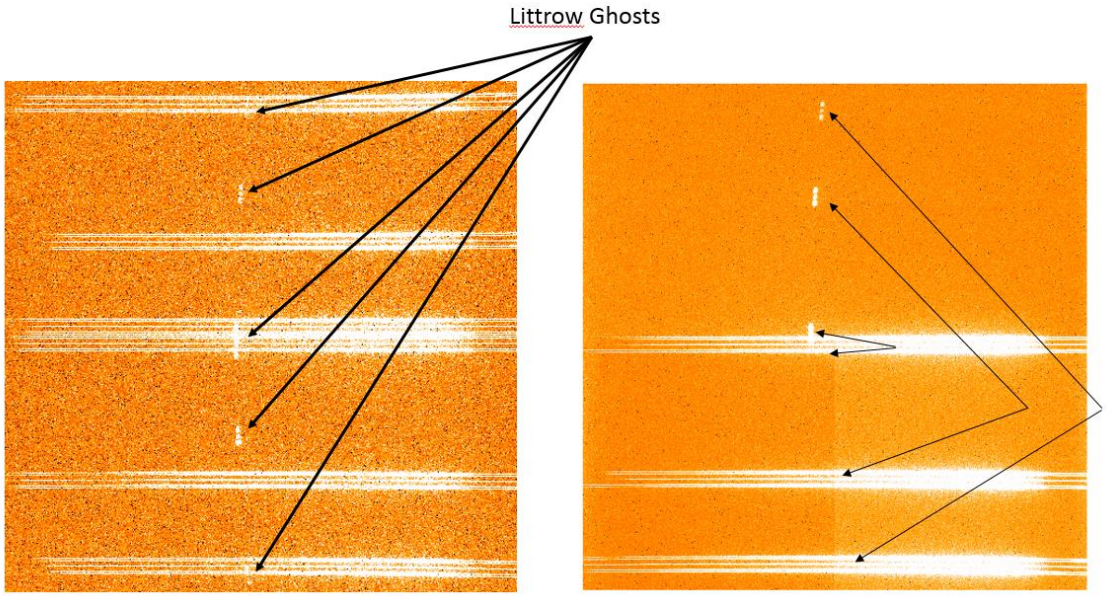

Figure 9. Littrow ghosts on the blue detector (contrast is enhanced). Associating each ghost to its parent image is easily done by illuminating only half a field as shown in the right.

4.6 Throughput

The absolute throughput measurement is performed on three wavelengths per channel. Flux level are measured at the Test Slit Unit exit and at each camera output: their ratio gives the LRS throughput excluding the slit lens and the field lens window, whose transmissions given by the manufacturer are then added to the measurements. Relative throughput measurements are deduced from the real CCD exposures with a continuum lamp.

The flux measurement tool is mainly based on an integrating sphere photodiode power sensor (with a wavelength range 350-1100 nm). The manufacturer ensures a linear response of the photodiode if the measured flux level is greater than 1µW. Such level cannot be achieved when illuminating the Test Slit Unit fibers with the Light Source Module used for the LRS alignment and test. Therefore a dedicated illumination unit (Figure 10), mounted at the QTH lamp exit, was developed to boost the flux injected into the fibers. Three interference filters are chosen for each channel, with transmission of at least 50% (>80% when available) and 10 nm bandwidth. Two more interference filters were used for the blue channel, to get measurement points at λ<400 nm. The filter bandwidth is constrained by the image size at the camera focus for the output flux measurement: 10 nm is the maximum bandwidth that ensures the whole flux to enter the photodiode integrating sphere. Only one slitlet at a time is illuminated, because the slit output beam size is too large and cannot be measured by placing a setup between the Slit Unit and the Collimator. The illumination unit injects light into the fiber bundle with an f-ratio of ~2.85, which can be reduced by limiting the aperture thanks to an iris diaphragm. Nevertheless, an f-ratio ratio greater than the one accepted by the LRS is kept for this measurement, because the flux level at f/3 is still not high enough for accurate measurements, especially in the blue wavelengths.

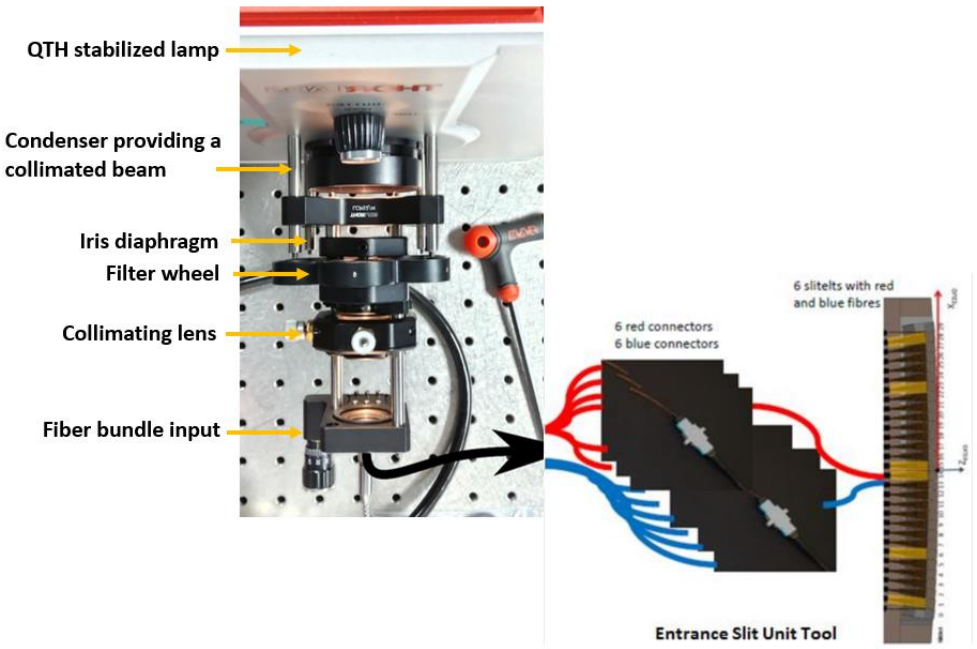

Figure 10. Illumination setup for absolute throughput measurement.

Input measurement setup:

A setup composed of two mirrors M1 and M2, chosen with a very high transmission (> 99%) is placed at the Test Slit Unit output and makes the slitlet output beam converge into the integrating sphere of the photodiode (see Figure 11). The most difficult part is to avoid the beam to be vignetted on M1. The illumination unit iris diaphragm aperture is thus adjusted to avoid any vignetting.

Two sets of mirrors are used: a first one with coatings optimized in the range 400-750 nm for the blue channel and green channels, and a second one with coatings optimized in the range 750-1100 nm for the red channel.

The measured input flux F_{in}^{meas} corresponds to the flux at the TSU exit, multiplied by M1 and M2 transmissions T_{M1} and T_{M2}. It is related to the LRS input flux F_{in} by correcting with the slitlens throughput $T_{slitlens}$:

$$F_{in} = \frac{F_{in}^{meas}}{T_{M1}T_{M2}T_{slitlens}} \quad (1)$$

T_{M1} and T_{M2} are given by the manufacturer and $T_{slitlens}$ is given by the silica transmission and AR coating properties provided by the slitlens manufacturer.

Output measurement setup:

The photodiode is placed at the camera focus and translation stages allowing displacement along the spectral, spatial and z optical axis directions allow to properly follow the curvature of the focal plane to ensure that the entirety of the flux enters the integrating sphere (see Figure 11).

A standard interface with the camera output holds the tool. The measured flux is related to the LRS output flux by correcting with the field lens window throughput:

$$F_{out} = F_{out}^{meas} T_{FLW} \quad (2)$$

T_{FLW} is given by the silica transmission and the AR coating properties provided by the manufacturer.

The LRS absolute throughput, at the given wavelength, is finally given by:

$$T_{LRS}(\lambda) = \frac{F_{out}}{F_{in}} \quad (3)$$

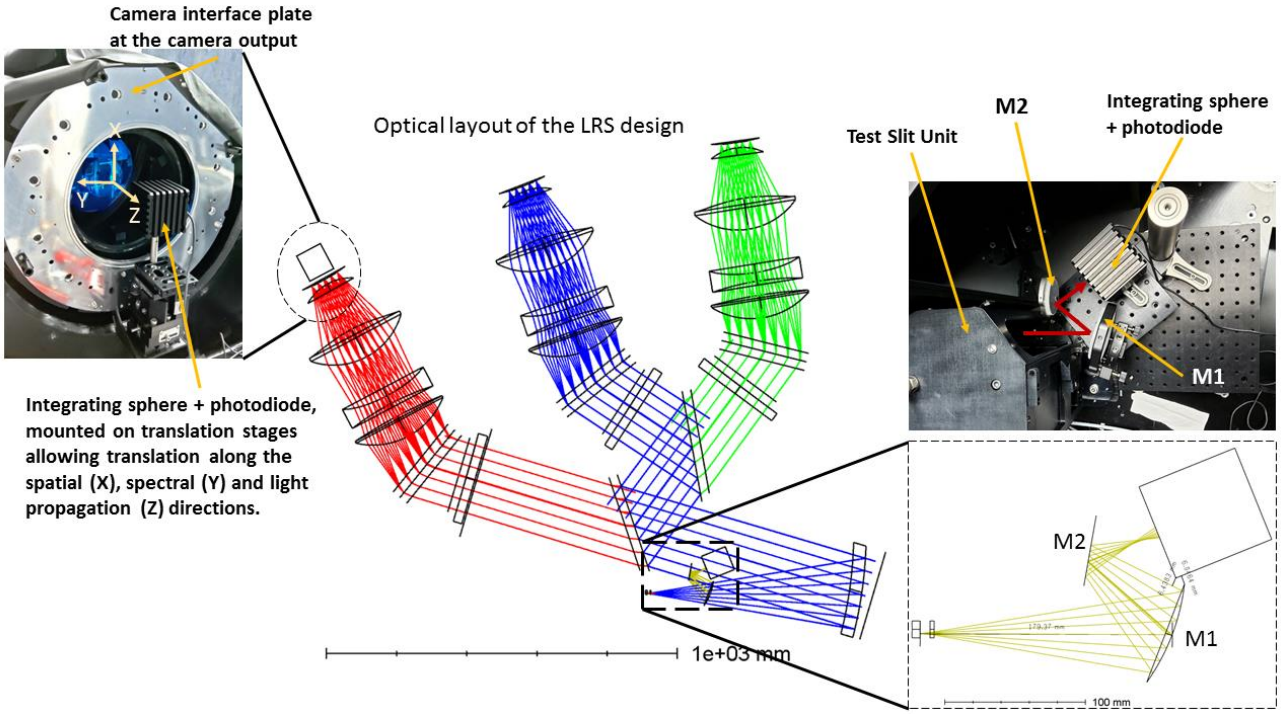

Figure 11. Throughput measurement setup.

Error bars associated to each measurement point are estimated thanks to coating properties of the different optics considered (M1, M2, slitlens and field lens window), as provided by the suppliers. It also takes into account the photodiode linearity and the continuum lamp stability, which we measured.

Relative throughput measurement:

- Output measurement: the output flux for each channel is calculated on real CCD exposures of the slit fibers illuminated with the continuum lamp. This flux in ADU/pix is converted into ADU/mm using the dispersion law. It has to be corrected from the detector efficiency to get the output flux at the Field Lens Window exit.
- Input measurement: the LRS Test Slit Unit fibers are illuminated thanks to the Light Source Module used for the LRS global tests and described in section 3. The LRS input flux is measured at the illumination unit exit (before injection into the fiber bundle) by recording a low resolution spectrum of the {Light Source + Liquid Light Guide + IU optics} thanks to a fiber coupled lab low resolution spectrometer. It was smoothed to reduce the noise level, which is especially high in the blue end of the range due to faint flux coming from the continuum lamp.
- Relative throughput curve: for each channel, the ratio of the output to the input spectrum, properly corrected for the detector and fiber transmission, gives the relative throughput over the wavelength range. The relative throughput curve is then rescaled using the absolute measurement points.

These absolute and relative measurements are gathered in Figure 12.

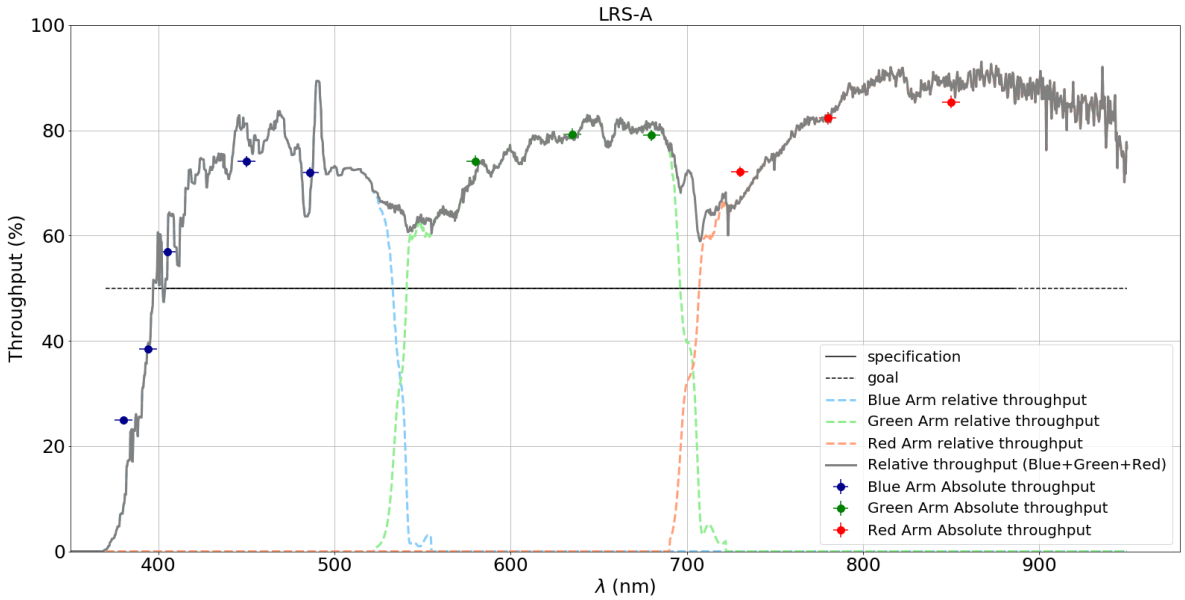

Figure 12. LRS throughput curve. The artefact around 480 nm on the relative throughput curve is due to internal calibration of the lab spectrometer used to measure the input spectrum.

4.7 Homogeneity of spectral response

Similarly to the relative flux transmission, the output flux for each channel is calculated on real CCD exposures of the slit fibers illuminated with the continuum lamp, and calibrated in wavelength using the dispersion law.

Fiber spectra are extracted and the output flux at a given wavelength between all illuminated fibers are compared, using the median value as a reference for comparison. Because the results would depend on the relative transmission of each fiber we consider only groups of 5 fibers (i.e. 1 slitlet) across the slit and compare each group of fiber providing the maximum flux.

Fiber-to-fiber variations appear and seem to correspond to variation of light injection into the fibers. To minimize the effect we combine 8 different exposures with the continuum lamp switching the 6 main fiber connectors into different

permutations. This provides enough statistics to minimize the fiber to fiber variations up to the TSU at each location of the slit.

The relative flux of each group of fibers (counted from 1 to 6) w.r.t the median flux of all fibers is shown for each channel in Figure 13. The horizontal dashed line shows the specified value (10%). Variations above 10% occur only below 400 nm and within the dichroic transition regions (524-554 nm and 691-721 nm).

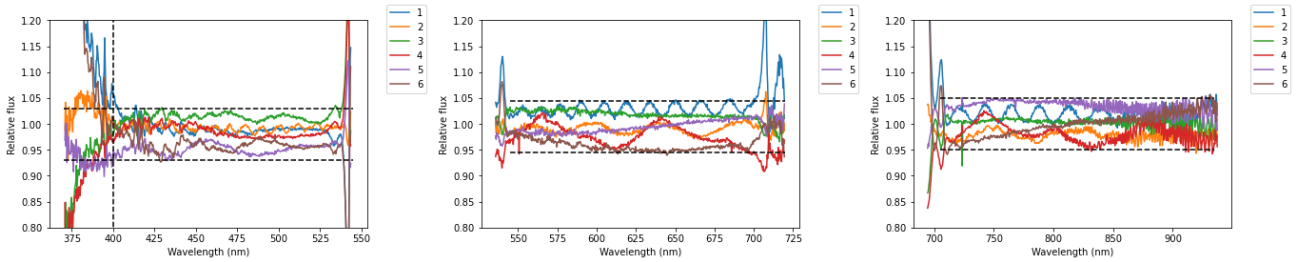

Figure 13. Relative fiber-to fiber transmission for the blue (left), green (middle) and red (right) channels.

4.8 Light Tightness

Each LRS is closed by a cover assembly ensuring light tightness, protection against dust and water during the instrument life time and thermal protection (it is expected to guarantee a stable temperature inside w.r.t environment temperature variations). It is composed of panels made of fiber glass epoxy and polyurethane foam for insulation, as well as EPDM foam gaskets for sealing.

In Lyon, the light tightness test was performed in the integration hall during the day with the lights on and by night with the light off to verify both specified background levels.

Dark exposures of 1 hour were taken and bias-subtracted with a master-bias. Only one dark was considered during the day while multiple dark exposures (up to 10) were taken during the night: in this case, averaging multiple exposures is necessary to lower the readout noise down to a negligible value compared to the measured signal, and this also helps better reject cosmic rays.

A cosmic ray rejection is performed by applying a median filter (especially useful when processing a single day time dark exposure). We measure the maximum value of these average 1 hour dark exposure over the full detector excluding the 100 pixels near the horizontal edges where glows are visible (mainly in the blue and green arms). We subtracted from this value the dark current of each detector provided by the manufacturer and ESO detector test results.

Results are shown in Figure 14 and Figure 15: maximum recorded values of dark level are compliant with the requirement (< 3e-/hour/pixel).

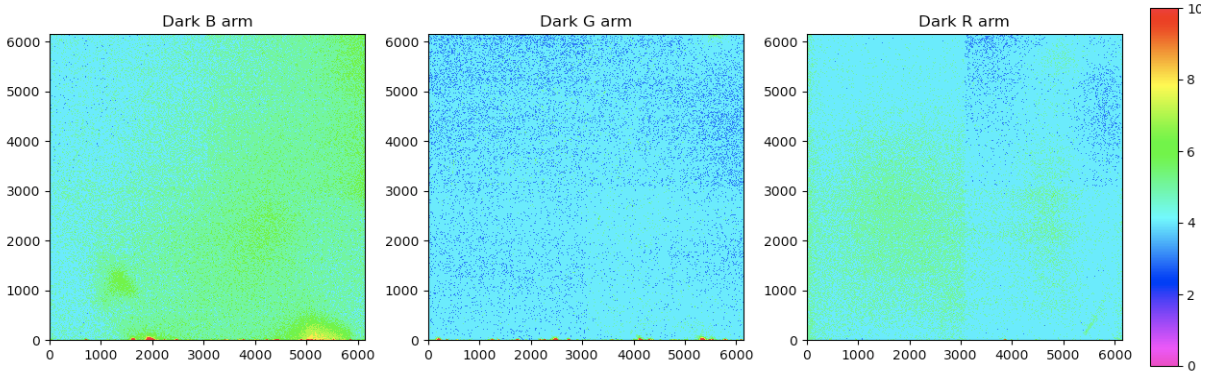

Figure 14. Day time dark exposure analysis (e-/hour/pixel). Maximum values are 8.0, 7.0 and 7.0 e-/hour/pixel in the blue, green and red channels respectively.

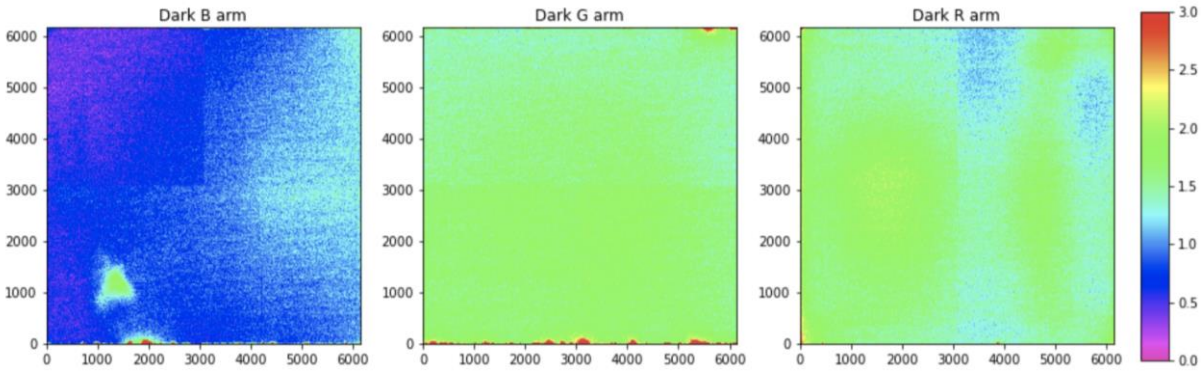

Figure 15. Night time dark exposure analysis (e-/hour/pixel). Maximum values are 2.3, 2.3 and 2.5 e-/hour/pixel in the blue, green and red channel respectively.

4.9 Spectrograph stability

The inner spectrograph temperature was regulated at 25°C. An arc exposure with Hg and Ne lamp is taken every half an hour with the full set of fibers illuminated. The environment (CRAL integration hall) temperature set point was regularly changed from 19°C to 25°C during the day. Therefore, the range of temperature difference between the inner LRS and the ambient environment varies between 0 and 6°C, which is smaller than the range in real operations (impossible to reproduce in practice in the integration hall). However, the dominant parameter for the observed displacements is the temporal variation of external temperature, which have been varied during the test to follow the same range observed at Paranal [10]. Therefore the results can be used directly to assess the stability in real operations.

All the exposures are bias-subtracted with a master-bias created at the beginning of the test. The position of each fiber on the CCD was computed for each exposure. Displacement of fiber core image is then processed using a cross correlation technique.

The results are shown in Figure 16 for each channel: the dX and dY fiber core displacement (in pixels) within an hour are plotted, and the color bar gives the external (ambient) temperature difference recorded within the hour between the two compared exposures. All points are required to enter the red circle showing the specification (1.5µm, i.e. 0.1 pixel, maximum displacement). The maximum displacement observed are 1.65, 1.95 and 2.1 µm for the blue, green and red channels respectively, with an estimated error of 0.3 µm. 3%, 7% and 8% of the points in the blue, green and red resp. are out of specification, and most of them are associated with a maximum external temperature variation greater than 1.5°C. When looking at the night temperature statistics at Paranal, such a temperature variation within one hour occurs during only ~5% of the nights.

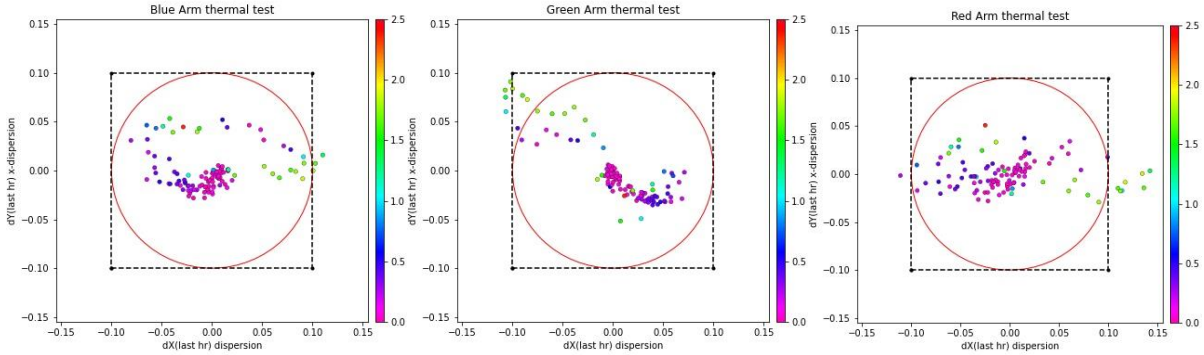

Figure 16. Fiber core displacement within an hour, in the blue (left), green (middle) and red (right) channels.

5. CONCLUSION

We demonstrated during the LRS test campaign at CRAL in our integration hall that the performances of the first spectrograph LRS-A were excellent and compliant with the requirements.
The LRS-A successfully passed its Local Acceptance Review in December, 2021, and was then disassembled and shipped to Potsdam, where it was re-integrated in March, 2022. Health-checks were performed after re-assembly: we verified mainly the performances related to image quality (spectral resolving power and sampling, spectral purity, cross-talk). They were found to be similar to the ones we obtained during the first integration, without any re-adjustment, proving the robustness of the opto-mechanical design and re-integration strategy.
We are currently carrying out the test campaign of the LRS-B. Thanks to the experience acquired with the LRS-A integration, we managed to even more finely adjust the positioning of every element, especially the detector vessel w.r.t the camera. Indeed, first results obtained on the blue channel show better results than for LRS-A in terms of image quality across the whole detector. We are now preparing for the local acceptance review of the LRS-B, planned in autumn, 2022.

We acknowledge the financial support of CRAL, CNRS, Université de Lyon, Université de Lyon 1 and LabEx Lyon Institut of Origins (LIO).

REFERENCES

[1] Roelof de Jong et al. “4MOST: the 4-metre multi-object spectroscopic telescope project in the assembly, integration and test phase” Proc SPIE 12184-40 (2022).
[2] Mark H. Cunningham et al., “The assembly and alignment of the 4MOST wide field corrector”, Proc SPIE 12184-257 (2022).
[3] Jurek Brzeski et al., “Overall performance of AESOP, the 4MOST fibre positioner”, Proc SPIE 12184-248 (2022).
[4] Andreas Kelz et al., “4MOST: manufacture, assembly and test of the optical fibre system”, Proc SPIE 12184-263 (2022)
[5] Walter Seifert et al., “4MOST: MAIT of the High Resolution Spectrograph”, Proc SPIE 12184-250 (2022)
[6] Patrick Caillier et al., “4MOST low resolution spectrograph final design”, Proc SPIE 10702-87 (2018)
[7] Steffen Frey et al., “4MOST preliminary instrument design”, Proc SPIE 9908-310 (2016)
[8] Olga Bellido et al., “4MOST systems engineering: from conceptual design to preliminary design review”, Proc SPIE 9911-76 (2016)
[9] Florence Laurent et al., “4MOST Low resolution spectrograph alignment”, Proc SPIE 12184-255 (2022)
[10] ESO ambient conditions database for the temperature at 2m level between 1996 and 2021 http://archive.eso.org/wdb/wdb/asm/meteo_paranal/form